

Invited paper

Recent advances in photodetectors with distributed optical amplification

Daniel Lasasa, Donato Pasquariello, Joachim Piprek, John E. Bowers

Electrical and Computer Engineering Department
University of California, Santa Barbara, CA 93106

ABSTRACT

For the past few years, we have been researching a novel type of photodetector featuring distributed optical amplification. We call these devices traveling-wave amplifier-photodetectors, or TAP detectors. The distributed combination of gain and absorption seeks a larger efficiency while keeping a low optical power, thus avoiding saturation. In this paper, we present experimental results both of GaAs- and InP-based TAP detectors, showing in the former case an external quantum efficiency larger than 200%, and larger than 100% in the latter. The performance limitation is shown to be related to the competition between the optical input signal and the amplified spontaneous emission (ASE) generated in the amplifier.

Keywords: photodetector, amplifier, distributed gain, GaAs, InP, efficiency, saturation.

1. INTRODUCTION

Photodetectors for optical communications should ideally exhibit large responsivity, large bandwidth, high saturation power and low noise. In order to improve the noise figure of photodetectors, the use of optical preamplification has been for a long time a usual technique. Integration of an electrically pumped semiconductor optical amplifier (SOA) together with a waveguide photodetector has yielded efficiency-bandwidth products in excess of 2THz [1]. This could significantly reduce both the production cost and the space occupied by receivers, eliminating the need for an erbium-doped fiber amplifier (EDFA) and its corresponding pump source, customarily used to provide optical preamplification. Research on integration of SOAs and photodetectors is of interest for various applications [2]. Recent advances on intermixing techniques [3], [4] further widen the horizon of possibilities for such integration.

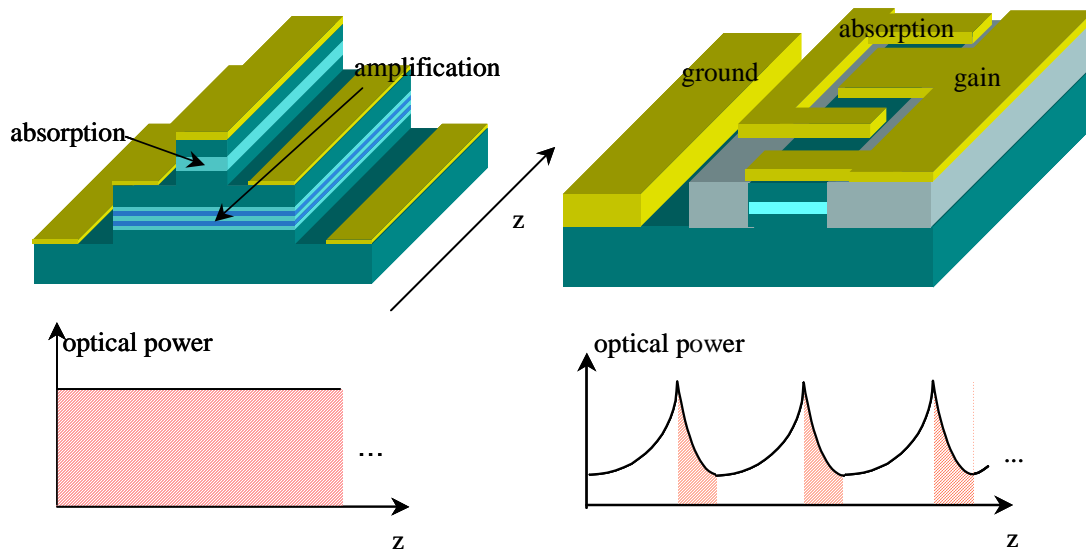


Figure 1: TAP detector configuration with vertical coupling (left) and with alternating gain and absorption (right). The graph shows the optical power evolution along the device. The shaded area is proportional to the generated photocurrent. With a limited optical power, large photocurrents are possible.

One of the main limitations for the previous approach stems from saturation, either in the detector or the amplifier. The maximum unsaturated photocurrent that may be extracted is no larger, in electrons per unit time, than the maximum amount of power that causes saturation in either the preamplifier or the photodetector, expressed in photons per unit time. Space-charge effects appearing in photodetectors may also seriously limit their high-frequency performance. In TAP detectors, the simultaneous or alternating combination of gain and absorption allows to keep a quasi-constant optical power while continuously generating photocurrent [5], [6]. This combination results in a larger efficiency for the same peak optical power. Figure 1 shows our two proposed configurations of TAP detectors.

In TAP detectors with transverse coupling, optical modes extend overlapping two active regions, one reverse-biased to provide gain, one forward-biased to provide absorption. When gain, absorption and loss exactly cancel out, an optical mode can propagate without its power changing, while continuously generating photocurrent. Transverse coupling may be achieved by combining gain and absorption regions laterally, or by stacking them vertically. The former was proposed in [5] and [6]. The latter is shown in Figure 1. Experimental results on TAP detectors with vertical coupling will be presented in this work.

TAP detectors with alternating gain and absorption present a single optical waveguide. Forward- and reverse-biased sections alternate in it, in the direction of light propagation. This results in the optical power being partially absorbed, then amplified before the next absorption section. When gain, absorption and loss in each period exactly cancel out, the power arriving to each detection section is the same, photocurrent being generated in all of them. The shaded area is proportional to the generated photocurrent, and can be very large in TAP detectors for a relatively low peak optical power.

A traveling-wave electrode structure may result in good high-frequency performance (>40GHz) for these devices. In the case of TAP detectors with alternating gain and absorption, impedance matching to 50Ω is also possible [6], as a result of the interconnection coplanar waveguide (CPW) presenting a combination of active and passive propagation sections.

In the following, we will present the fabrication process and experimental results of TAP detectors with vertical coupling. In section 5, the performance results obtained up to date will be discussed. Proposed alternatives to overcome the device limitations observed up to date will follow.

2. DEVICE DESIGN AND FABRICATION

TAP detectors with vertical coupling present two active regions stacked vertically. In our proposed configuration, the top active region is made of bulk material, reverse-biased for absorption, as shown in Figure 2. The bottom active region presents multiple quantum-wells (MQWs), and is forward-biased to provide optical gain. This ability to optimize separately the active regions for gain and absorption is one of the advantages of the configuration presenting vertical coupling. Another advantage of this configuration with vertical coupling is the presence of a good electrical isolation without the need of an elaborate scheme of ion implantation and/or regrowth. The experimental results shown in this paper were all obtained from single epitaxy material.

Key issues that need to be considered for optimum device performance are the existence of a background current, arising in the detector by reasons other than the absorption of amplified input signal, and the overlap between the optical modes with both active regions. A brief discussion of the roles of these factors, and the design rules obtained from detailed simulations follows [7]-[10].

2.1. Background current

The background current that will exist independently of an optical input has mainly three sources. First, reverse-biased diodes exhibit always a non-zero current flow. Next, the imperfect electrical isolation between gain and absorption diodes allows for current flow between them. This current flow may be added to the photocurrent. Finally, ASE generated in the gain region is detected in the absorption region. The latter contribution will be therefore called ASE photocurrent, and will be shown by experiment to dominate the background current, and to have important repercussions in the device behavior.

Electrical isolation between both active regions is very important for optimum device performance. Otherwise, strong electrical current may flow between the gain and absorption diodes. This current will add to the detector current, as well as removing part of the carriers injected to pump the gain region. In TAP detectors with vertical coupling, the main contribution to this dark current will stem from a parasitic transistor formed by the cladding layer of both active regions. Let us assume that the conductive layers between both active regions (middle cladding) are n-doped, and the

layers below the amplifier region (bottom cladding) and above the detector (top cladding) are p-doped. Thus, a p-n-p transistor is formed, the emitter being the bottom cladding, the base the middle cladding and the collector the top cladding. This is schematically represented in Figure 2.

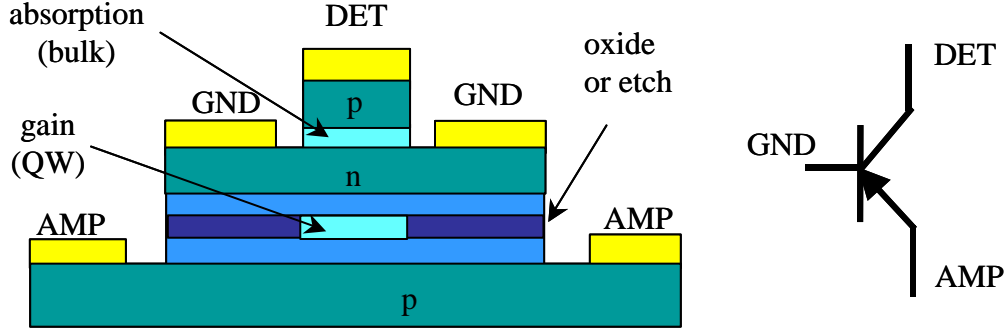


Figure 2: Schematic cross-section of a TAP detector with vertical coupling (left) and parasitic transistor (right). The contacts in the TAP detector and the corresponding terminals in the transistor are labeled identically for clarity.

The holes injected from the bottom region, in order to arrive at the middle cladding (base) need to travel through the amplifier active region. The presence of the QWs, together with the separate confinement heterostructure (SCH) barrier, makes this transit difficult. The thickness of the middle cladding is another obstacle for the electrons to arrive to the collector (top cladding), or even to the intrinsic absorption region. Finally, in the case of GaAs-based devices, high Al-content layers were grown above and below the gain region. Their purpose was to confine both the amplifier bias current and the optical mode through lateral oxidation. This results in an increased carrier density (and thus increased gain) for the same bias current, and in a reduction of the number of lateral modes. These layers were doped, presenting no obstacle to the injection of current into the gain active region. A large barrier appears to carriers trying to leave the amplifier region. The experimental data showed later on will show that, overall, the effect of the parasitic transistor can be neglected in GaAs-based devices, appearing in InP-based devices only at very high (~100mA) current injection into the amplifier. We believe that the high Al-content layers are responsible for this difference in the device behavior.

2.2. Overlap between the optical mode and the active regions

As discussed in previous work [5], [6], optimum performance avoiding saturation requires that optical gain, absorption and loss are close to cancellation. Given the usual values for bulk material absorption and quantum-well material gain [7], this requires a confinement factor about 4 times larger in the gain region than in the detection region. A larger overlap with the absorption region would result in the input optical power being quickly attenuated, thus not benefiting from the distributed combination of absorption and gain. A small overlap with the absorption region would result in a mode that would increase rapidly, thus contributing to gain saturation, while not contributing significantly to the total photocurrent. Such a mode existed in the first generation of GaAs-based TAP detectors, whose performance is discussed in [8]. We believe that this mode was responsible for limiting the device performance of that generation.

Different modes will exhibit different confinement factors in both active regions. It is therefore close to impossible to ensure that all modes will satisfy simultaneously this condition. Selective undercut etch in InP-based devices and oxidation in GaAs-based devices provide also lateral optical confinement, thus reducing the number of undesired modes. If the amplifier active region was much wider than the detector region, such lateral modes might reside mostly in the amplifier, resulting in a similar effect as observed in the first generation of GaAs-based TAP detectors. Detailed simulations were performed to ensure that the laterally confined modes would exhibit the appropriate confinement factors [7], [8].

2.3. Optimized GaAs-based structure.

The InP-based material used to obtain higher than 100% external quantum efficiency is described in detail in [10]. We will therefore present now only the optimized GaAs structure, since some variations were introduced with respect to the one proposed in [8]. In that work, a $\text{Al}_{0.35}\text{Ga}_{0.65}\text{As}$ composition was assigned to the bottom p-doped contact and to the semi-insulating (SI) sublayer. This provided confinement factors of ~19% and ~5.6% in the amplification and

absorption regions, respectively. However, this composition is not entirely realistic, since it presents high resistance even with high doping, due to the migration of a large fraction of the electrons from the Γ valley to the X valley in the conduction band. Due to this necessary change in composition, the SCH needed to be widened in order to obtain a propagating mode with similar confinement factors with the gain and absorption region. Their respective values, for the structure shown in Table 1, were 16% and 3.7%. The coupling efficiency from a fiber into this mode is simulated to be 48%. All other propagating modes found for this structure had larger confinement factors in the absorption region and lower confinement factors in the absorption region. When gain, absorption and loss cancel for the described mode, all other modes will vanish after a certain distance.

Layer name	Thickness	Composition	Doping
absorption	200nm	GaAs	
contact (n)	100nm	$\text{Al}_{0.15}\text{Ga}_{0.85}\text{As}$	$5 \cdot 10^{18}$
cladding (n)	600nm	$\text{Al}_{0.2}\text{Ga}_{0.8}\text{As}$	$1 \cdot 10^{18}$
parabolic grade (n)	16.5nm	$\text{Al}_{0.2}\text{Ga}_{0.8}\text{As}$ to $\text{Al}_{0.9}\text{Ga}_{0.1}\text{As}$	$1 \cdot 10^{18}$
Oxidation layers (n)	6nm	$\text{Al}_{0.9}\text{Ga}_{0.1}\text{As}$	$1 \cdot 10^{18}$
Oxidation layers (n)	32nm	$\text{Al}_{0.98}\text{Ga}_{0.02}\text{As}$	$1 \cdot 10^{18}$
Oxidation layers (n)	6nm	$\text{Al}_{0.9}\text{Ga}_{0.1}\text{As}$	$1 \cdot 10^{18}$
parabolic grade (n)	18.2nm	$\text{Al}_{0.9}\text{Ga}_{0.1}\text{As}$ to $\text{Al}_{0.15}\text{Ga}_{0.85}\text{As}$	$1 \cdot 10^{18}$
SCH (n)	140nm	$\text{Al}_{0.15}\text{Ga}_{0.85}\text{As}$	$1 \cdot 10^{18}$
SCH	10nm	$\text{Al}_{0.15}\text{Ga}_{0.85}\text{As}$	
7QW	8nm	GaAs	
barrier	8nm	$\text{Al}_{0.15}\text{Ga}_{0.85}\text{As}$	
SCH	60nm	$\text{Al}_{0.15}\text{Ga}_{0.85}\text{As}$	
SCH (p)	90nm	$\text{Al}_{0.15}\text{Ga}_{0.85}\text{As}$	$5 \cdot 10^{17}$
parabolic grade (p)	18.2nm	$\text{Al}_{0.2}\text{Ga}_{0.8}\text{As}$ to $\text{Al}_{0.9}\text{Ga}_{0.1}\text{As}$	$1 \cdot 10^{18}$
Oxidation layers (p)	6nm	$\text{Al}_{0.9}\text{Ga}_{0.1}\text{As}$	$3 \cdot 10^{17}$
Oxidation layers (p)	32nm	$\text{Al}_{0.98}\text{Ga}_{0.02}\text{As}$	$3 \cdot 10^{17}$
Oxidation layers (p)	6nm	$\text{Al}_{0.9}\text{Ga}_{0.1}\text{As}$	$3 \cdot 10^{17}$
parabolic grade (p)	16.5nm	$\text{Al}_{0.9}\text{Ga}_{0.1}\text{As}$ to $\text{Al}_{0.25}\text{Ga}_{0.75}\text{As}$	$2 \cdot 10^{18}$
spacer (p-doped)	300nm	$\text{Al}_{0.25}\text{Ga}_{0.75}\text{As}$	$5 \cdot 10^{17}$
contact (p-doped)	200nm	$\text{Al}_{0.25}\text{Ga}_{0.75}\text{As}$	$5 \cdot 10^{18}$
Cladding (p-doped)	200nm	$\text{Al}_{0.25}\text{Ga}_{0.75}\text{As}$	$2 \cdot 10^{18}$
sublayer (SI)	$3\mu\text{m}$	$\text{Al}_{0.25}\text{Ga}_{0.75}\text{As}$	SI
substrate (SI)	$\sim 150\mu\text{m}$	GaAs	SI

Table 1: Single epitaxy structure for optimized GaAs-based TAP detectors with vertical coupling.

Simulations and optimized epitaxial structure for InP TAP detectors are presented in [10]. We will therefore not discuss them further here.

3. DEVICE FABRICATION

In this section, the fabrication process used to produce TAP detectors with vertical coupling is briefly described. Special attention will be paid to possible problems during the fabrication and the solutions implemented.

3.1. Fabrication of GaAs-based TAP detectors.

GaAs-based TAP detector fabrication starts with the lift-off deposition of Ti/Pt/Au contacts to provide a Schottky contact to the bulk intrinsic absorption region. Using this metal as a mask, the intrinsic region is etched, using a $\text{H}_2\text{SO}_4:\text{H}_2\text{O}_2:\text{H}_2\text{O}$ (1:4:40) solution. Next, Ni/AuGe/Ni/Au contacts to the intermediate n-cladding layer are deposited, and annealed at 420°C . The amplifier waveguide is etch using Cl_2 reactive ion etching. The contact to the p-doped bottom cladding is evaporated next, using Pd/Zn/Pd/Au, and subsequently annealed at 380°C . Wet oxidation at 400°C

follows. 10 liters per minute of N_2 pass through a bubbler containing water at $90^\circ C$ during this step. The devices are planarized using PMGI. Finally, thick Au interconnection CPW and gain pads are deposited, using Ti as a sticking layer. In early attempts to produce TAP detectors, it was noted that oxidation at temperatures of $420^\circ C$ and higher resulted in the gain diodes being shorted. We believe that gold spiking through the middle cladding is responsible for this. Subsequently, oxidation was performed always at $400^\circ C$. Any other thermal process, including contact alloying, was kept at a temperature as low as possible. After these changes were introduced in the fabrication process, the phenomenon was not observed again.

Although Ti/Pt/Au or Cr/AuZn/Cr/Au are usual metal schemes to create ohmic contacts on p-GaAs, the high Al content (25%) of the bottom cladding in our device design produces a small voltage drop when these alloys are used, and relatively high ($\sim 10^{-5} \Omega cm^2$) residual contact resistance, for annealing temperatures up to $440^\circ C$. Pd/Zn/Pd/Au produces however ohmic contacts even as deposited. Annealing at $380^\circ C$ is enough to provide good contact resistance ($\sim 10^{-6} \Omega cm^2$). No significant improvement was observed at higher temperatures.

Figure 3 shows pictures of fabricated TAP detectors. Note that the devices are staggered, so that with one cleave TAP detectors of different lengths are produced.

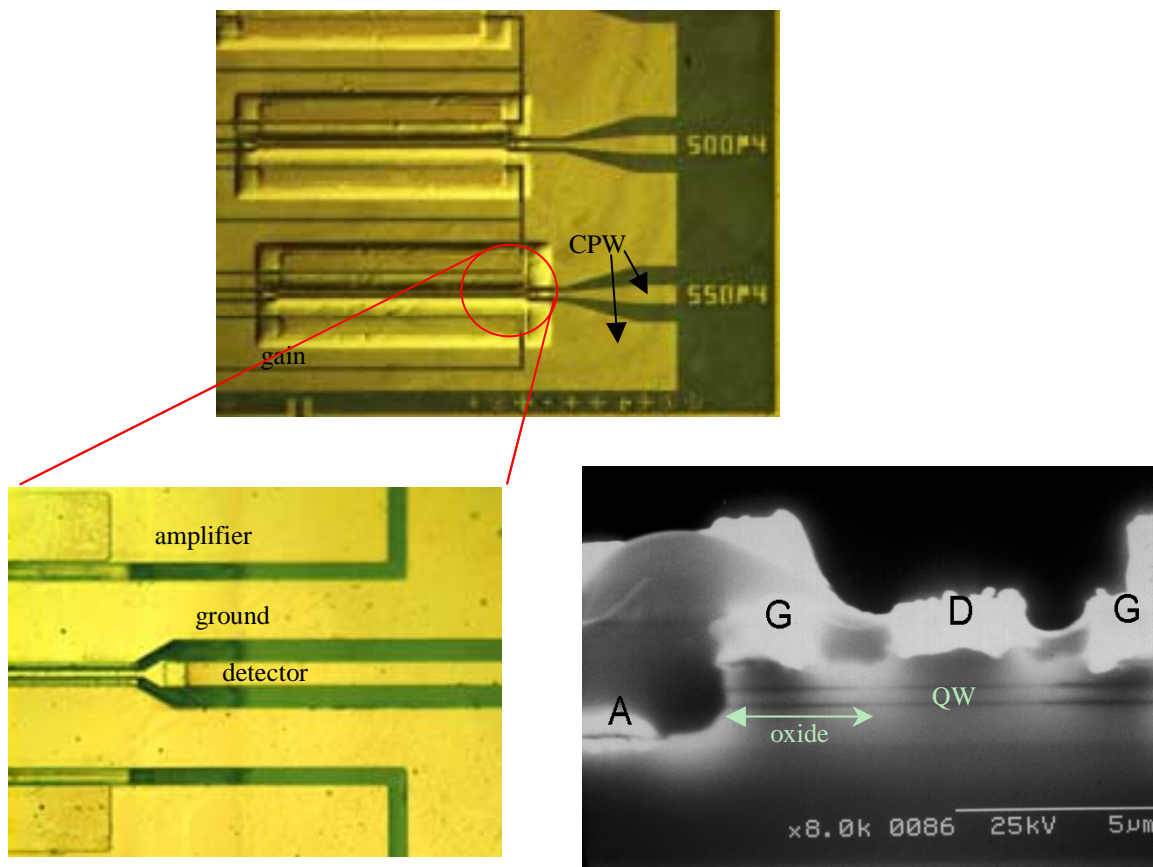


Figure 3: Top view (top) and detail (bottom left) of TAP detectors fabricated in GaAs. The SEM micrograph (bottom right) shows the device cross-section at the input facet. Oxide for lateral confinement may be appreciated as a darker layer. Contacts are labeled D for detection region, A for amplification, and G (ground) for the middle cladding.

The devices fabricated were measured before and after deposition of a 1200 \AA SiO_x anti-reflection (AR) coating. Residual reflection after AR-coating the device input facet was estimated to be below 1%.

3.2. Fabrication of InP-based TAP detectors.

The procedure to fabricate InP-based TAP detectors is now briefly described. Ohmic contacts for the absorption region are deposited by lift-off, using a Ti/Pt/Au metal scheme, and subsequently annealed at 410°C. The absorption region is then etched by CH₄:H₂:O₂ reactive ion etching using this metal as a mask. SiN_x is then deposited via PECVD, both to serve as a mask for the amplification region etch, and for protection of the laterally exposed top n-doped contact layer. After etching the middle cladding layer, a new SiN_x PECVD deposition protects the exposed middle cladding p-doped contact layer. The amplifier region is then etched. Subsequently, lateral undercut wet etch defines the gain active region. A H₂SO₄:H₂O₂ solution provides great selectivity between the gain region and the rest of the material. PECVD deposited SiO₂ provides mechanical support for the laterally undercut material. Ohmic contacts to the middle p-doped cladding are then deposited, using Ni/AuGe/Ni/Au. A new Pd/Zn/Pd/Au evaporation forms the contact to the bottom n-doped cladding. Finally, the devices are planarized using PMGI, and the interconnection CPW is deposited. After cleaving, a 2200Å SiO_x AR coating reduces the input facet reflectivity to less than 1%.

In the first generation of InP-based TAP detectors, it was found that the rate of the lateral undercut etch was extremely difficult to control in the presence of metal deposited to provide ohmic contacts to the middle cladding. In subsequent generations, this metal was therefore deposited after the undercut etch had been performed.

Application of bias to the amplifier would sometimes result in collapse of the laterally undercut region. PECVD deposited SiO₂ proved to provide extra mechanical support, reducing greatly the frequency of this collapse. Figure 4 shows pictures of TAP detectors fabricated in InP.

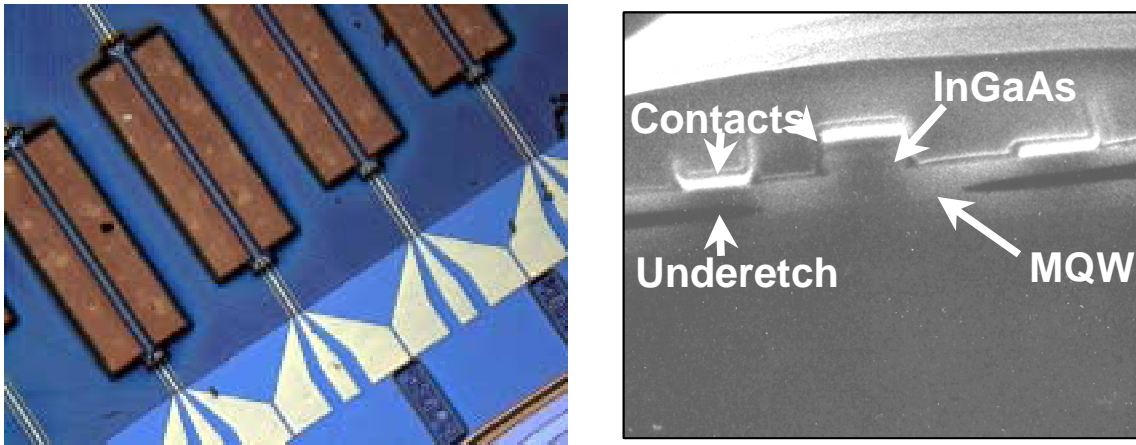


Figure 4: Pictures of TAP detectors fabricated in InP. Top view (left) and SEM micrograph detail of the input facet (right). The laterally undercut region is clearly shown in the latter.

4. EXPERIMENTAL RESULTS

In order to fully characterize and understand the behavior of TAP detectors, several different measurement results will be presented. Their purpose is not only to show the proof of principle behind these devices, and their external quantum efficiency higher than 100%, but also to understand the reasons for the performance values obtained, and how to improve them further in the future. After a quick description of the measurement setup, results of GaAs-based TAP detectors will be presented, then results from InP-based devices. In both cases, we will first characterize the background current. We will show how most of it comes from absorption in the detection region of ASE generated in the gain region, to the point where the effect of the parasitic transistor may be neglected in most cases. Next, results under incident optical input will be presented. They will constitute proof that the distributed combination of amplification and absorption is indeed capable of producing external quantum efficiency larger than 100%. In the case of GaAs-based TAP detectors, measurements of stray spontaneous emission generated in the gain region are also shown.

4.1. Measurement setup

The experimental setup used to characterize the performance of TAP detectors in the absence of input signal is schematically presented in Figure 5. An HP-4145 semiconductor parameter analyzer is used both as a current source for the gain diode and a voltage source and current meter for the absorption diode. The ASE emitted from the input facet is measured by means of an external broad-area detector. A second broad-area detector is used to collect stray spontaneous emission leaving the gain region. This second detector is positioned in a plane perpendicular to the direction of propagation, and at an angle of $\sim 45^\circ$ with respect to the sample top surface. With this arrangement we minimize the contribution from any source other than non-amplified spontaneous emission. The copper stage over which the devices were probed was temperature-stabilized at room temperature by using a thermoelectric cooler.

TAP detector performance in the presence of light illumination was characterized by substituting the broad area detector collecting the ASE by a lensed fiber, in order to optimize the input coupling. The background current was measured first, in the absence of light input. An optical signal was then coupled into the device, and the total current in the presence of light input was measured. The photocurrent was obtained by subtracting both values. The results obtained with this setup will be presented next.

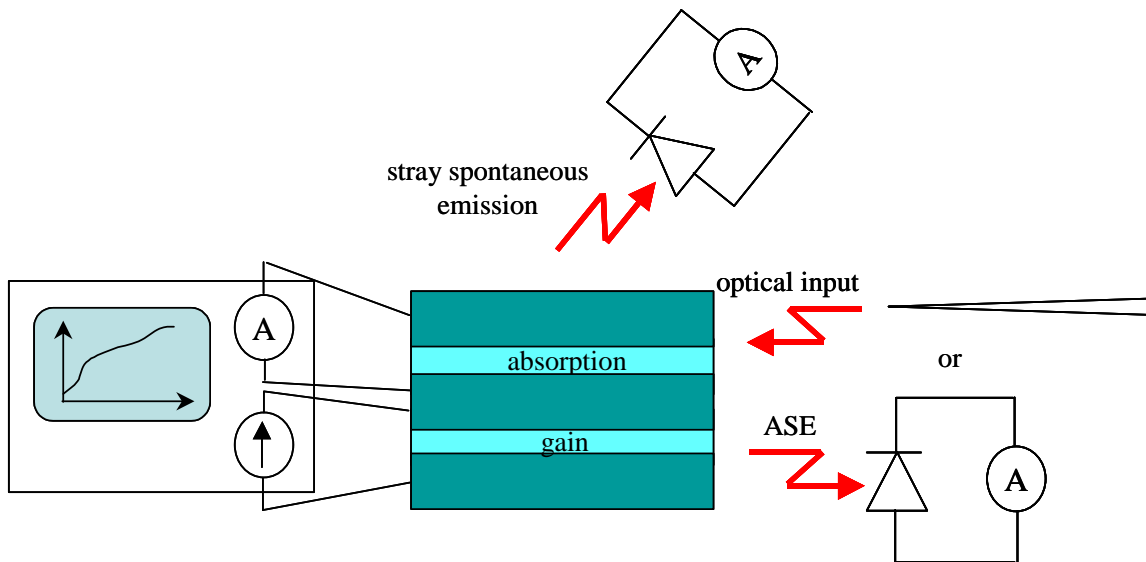


Figure 5: Schematic of the experimental setup for the characterization of vertically coupled TAP detectors. The background current in the absorption region may be measured simultaneously as the ASE output of the device and the stray spontaneous emission produced in the gain current. Using a lensed fiber, light input may be introduced. We can then measure the total current generated in the absorption region and at the same time the stray spontaneous emission.

4.2. Experimental characterization of GaAs-based TAP detectors

Results corresponding to a $200\mu\text{m}$ long, $3\mu\text{m}$ wide TAP detector fabricated out of the epitaxial structure described in table 1 will now be presented. Figure 6 shows the background current across the absorption diode, together with the ASE coupled out of the device input facet, and the stray spontaneous emission. It is interesting to note that the ASE power and the background current follow the same trend. This seems to point to the fact that most of the contribution to the dark current stems from absorption of ASE generated in the gain region. It also strongly suggests that the effect of the parasitic transistor shown in Figure 2 can be neglected in these devices.

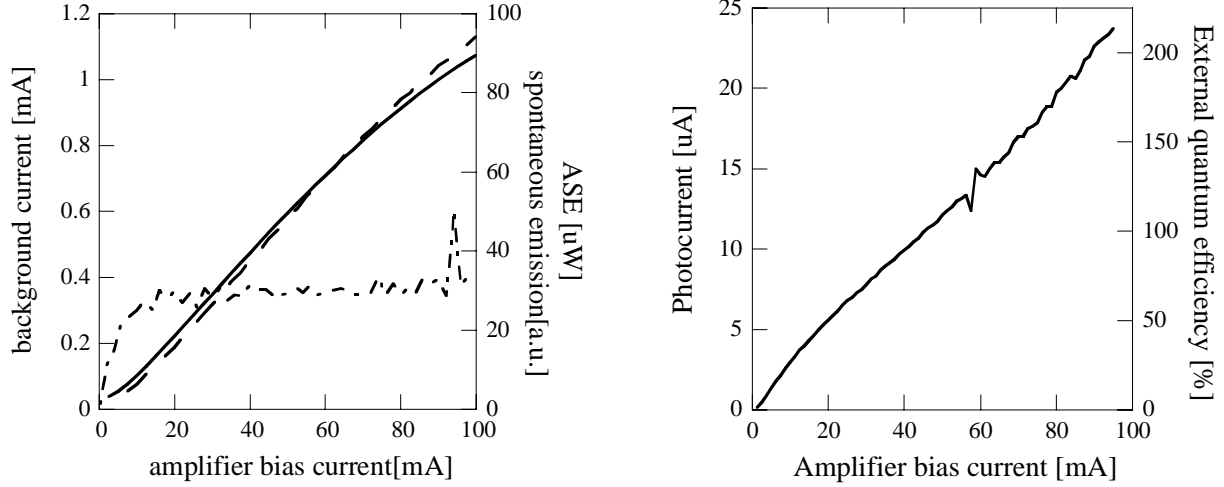


Figure 6: Left: the background current in GaAs-based TAP detectors (full line) and the ASE coupled out of the input facet (dashed line) follow the same trend. The spontaneous emission generated in the gain region (dash-dotted line) seems to increase very slowly with amplifier bias, suggesting a slow change in carrier density with increasing bias current. Right: measured photocurrent for an input of $16\mu\text{W}$, corresponding to external quantum efficiency in excess of 200%.

The stray spontaneous emission shows a quick initial growth, followed by a much slower increase with amplifier bias current. This shows that the spontaneous emission that does not couple into a propagating mode in the device does not play a substantial role in the generation of the background current. It also shows that the carrier concentration in the gain region increases slowly with the amplifier bias current.

Figure 6 shows also the measured photocurrent for an input power of $16\mu\text{W}$, at a wavelength of 860nm (coinciding with the peak of the gain). The corresponding external quantum efficiency reaches values over 200%.

4.3. Experimental characterization of InP-based TAP detectors

Results corresponding to a $3\mu\text{m}$ wide, $300\mu\text{m}$ long InP-based TAP detector will be presented next. Figure 7 shows the background current, and the spontaneous emission coupled out of the device, as a function of bias current. They are shown to follow basically the same trend, except at very large amplifier bias currents. At this point, the background current seems to stay close to constant even though the ASE starts rolling off because of heating. This is most probably some residual effect from the parasitic transistor shown in Figure 2. Note that the effect is still minimum.

Figure 7 shows also the responsivity and external quantum efficiency for these devices, for an input signal wavelength of $1.55\mu\text{m}$. The latter is in excess of 100%.

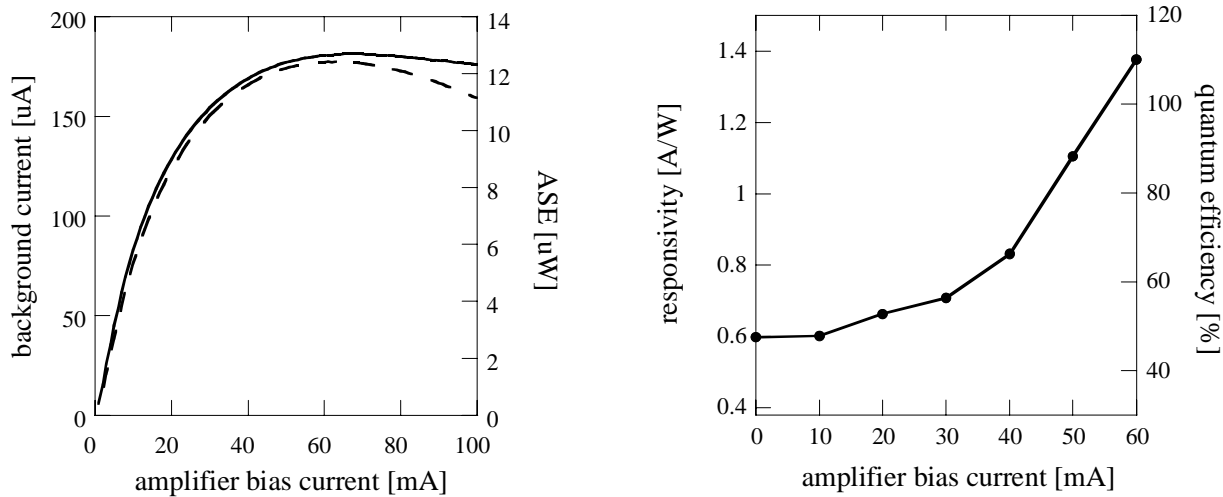


Figure 7: Left: the background current in In-P TAP detectors (full line) and the ASE coupled out of the input facet (dashed line) follow the same trend. At very high amplifier bias, some residual effect from the parasitic transistor may be observed. Right: responsivity measured for an input of $2.1\mu\text{W}$, corresponding to an external quantum efficiency in excess of 100%.

5. DISCUSSION

The results presented constitute proof of principle that the distributed combination of amplification and absorption may result in devices with external quantum efficiency higher than 100%. To our knowledge, our work constitutes the first successful implementation of distributed gain and absorption. The next question is, of course, what are the fundamental limitations of this technique, and what factors are currently limiting TAP detector performance. Figure 8 may contain the key to answering those questions. The curves shown are the background current generated by absorption of ASE in the absence and in the presence of an input signal, and total current in the presence of the same input.

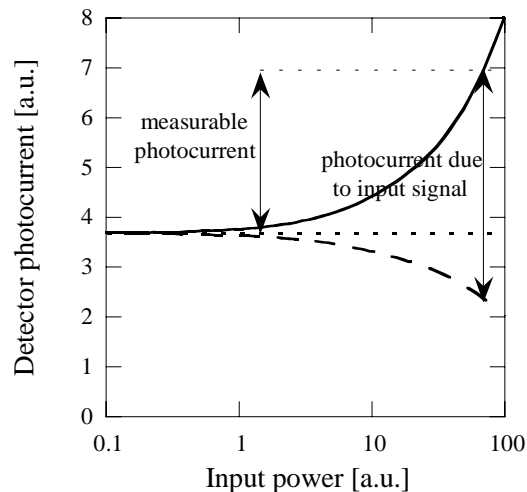


Figure 8: In the presence of an optical signal, the ASE generated in the amplifier is reduced, resulting in a lower background current (dashed line). The photocurrent actually generated by amplification and absorption of the input signal is higher than the difference between the total current in the presence of an input (full line) and the background current in the absence of said input.

The data shown in Figure 8 were obtained by taking into account the different processes that generate or annihilate electrical carriers in the gain region. In steady state operation, the amount of carriers injected by electrical pumping and generated via stimulated absorption of light, per unit time, must be equal to the number of carriers that recombine non-radiatively, or producing spontaneous or stimulated emission of light. As the optical power in the device increases (i.e., as we couple into it more optical power), the stimulated emission and absorption rates increase. If the device is biased at a point where the gain region is providing net gain, the former will dominate. If the current injected remains constant, other annihilation terms need to decrease. The carrier density in equilibrium must therefore be smaller as the input optical power increases. This results, obviously, in lower ASE power generation, and consequently lower background current, as expressed in Figure 8. In conclusion, the measurable photocurrent, i.e., the difference between the total current in the presence of an input signal, and the background current in the absence of a signal, is actually smaller than the photocurrent generated by the amplification and absorption of the input signal. Thus, the competition for the available electron-hole pairs between the ASE and the input signal results in an apparent device saturation. This theory is reinforced by Figure 6, which shows that the spontaneous emission remains mostly constant, whereas the ASE power increases. This shows that the dominating recombination term, in the absence of an input signal, is the stimulated emission of photons providing gain to the ASE, since extra carriers injected by an increase in the bias current result in a larger ASE, but not in an appreciably larger spontaneous emission.

In the case of TAP detectors, the effect of ASE is more important than in SOAs, for two reasons. First, not only the forward-propagating ASE contributes to the background current, but also the backward-propagating ASE. Second, in the configuration presented in this paper, there is no filtering of the ASE between the amplification and the absorption regions. Thus, all ASE from the entire amplifier bandwidth contributes to the total background current. Note however that, in the case where spontaneous emission of photons (which we have shown not to have a measurable impact on the background current), or non-radiative processes, were the dominating recombination mechanisms, a reduction in the carrier density would not necessarily result in a lower background current, or at least not in an important enough reduction in it. The competition between input signal and ASE must therefore be avoided.

To conclude this short discussion, we may point first that the actual photocurrent generated by the signal may be higher than the one that we have measured. A careful study of the competition between ASE and input signal needs therefore to be carried out. Second, as a guideline for future work, we suggest the study and fabrication of TAP detectors with alternating gain and absorption. The current state of the art makes these devices feasible now [3], [4], and they allow the possibility of introducing, between the regions providing gain and absorption, of wavelength-selective loss. This could be doable, for example, by intermixing the same quantum-wells present in the amplification region, and reverse-biasing them. Thus, using the Franz-Keldysh effect, additional loss may be introduced at wavelengths shorter than the input signal wavelength. This could have multiple benefits. First, the extra loss would result in the ASE growing slower than the signal, and the recombination rate stimulated by already existing ASE would decrease. Second, the background current would decrease, resulting also in a lower noise figure. Finally, a decrease in the carrier density produced by the recombination events stimulated by the input signal would not have such a dramatic effect in the background current.

6. CONCLUSION

In conclusion, we have presented in this paper characterization of a novel type of devices, the traveling-wave amplifier-photodetectors, or TAP detectors. External quantum efficiencies higher than 200% have been demonstrated in GaAs-based devices, and higher than 100% in InP-based devices. The competition between signal and ASE for the available electron-hole pairs, and thus for the available optical gain, has been suggested as the main limiting factor of TAP detector performance up to date. Strategies have been proposed to overcome this limitation.

7. REFERENCES

1. Wake, D., "A 1550-nm millimeter wave photodetector with a bandwidth-efficiency product of 2.4THz," *Journal of Lightwave Technology*, vol. 10, n. 7, pp. 908-12, 1992.
2. Fengnian, X, Wei, J., Menon, V., Forrest, S.R., "Monolithic integration of a semiconductor optical amplifier and a high bandwidth p-i-n photodiode using asymmetric twin-waveguide technology," *IEEE Photonics Technology Letters*, vol. 15, no. 3, pp. 452-4, 2003.

3. Skogen, E.J., Barton J.S., Denbaars, S.P., Coldren, L.A., "A quantum-well-intermixing process for wavelength-agile photonic integrated circuits," *IEEE Journal of Selected Topics in Quantum Electronics*, vol. 8, no. 4, pp. 863-9, 2002.
4. Skogen, E.J., Barton J.S., Masanovic, M.L., Getty, J.T., Denbaars, S.P., Coldren, L.A., "Use of post-growth control of the quantum-well band edge for optimized widely-tunable laser-x devices," *2002 IEEE 18th International Laser Conference Digest*, pp. 53-4, 2002.
5. Lasaos, D., Chiu, Y.J., Piprek, J., Bowers, J.E., "Traveling-wave amplification photodetectors (TAP detectors)," *Proceedings of the 2000 IEEE Lasers and Electro-Optics Society 13th Annual Meeting*, vol 1, pp. 260-1, 2000.
6. Lasaos, D., Chiu, Y.J., Piprek, J., Bowers, J.E., "Modeling of traveling-wave amplification photodetectors (TAP detectors)," *Proceedings of the SPIE Photonics West Conference*, vol. 4283, pp. 528-39, 2001.
7. Piprek, J., "Semiconductor optoelectronic devices – Introduction to physics and simulation," ch. 11, *Academic Press*, 2003.
8. Piprek, J., Lasaos, D., Pasquariello, D., Bowers, J.E., "Optimization of GaAs amplification photodetectors for 700% quantum efficiency," *IEEE Journal of Selected Topics in Quantum Electronics*, vol. 9, 2003 (to be published).
9. Piprek, J., Pasquariello, D., Lasaos, D., Bowers, J.E., "1.55 micron traveling-wave amplification photodetector," *Proceedings of the IEEE Conference on InP and Related Materials – IPRM*, pp. 499-501, 2003.
10. Pasquariello, D., Piprek, J., Lasaos, D., Bowers, J.E., "InP-based waveguide photodetector with integrated photon multiplication," *Proceedings of the SPIE ITCOM Symposium, Semiconductor Optoelectronic Devices for Lightwave Communication*, vol. 5248 (to be published).